Available online at www.sciencedirect.com

SciVerse ScienceDirect

Acta Materialia 61 (2013) 4910–4919

Acta MATERIALIA

www.elsevier.com/locate/actamat

# Microstructure control of unidirectional growth of η-$Cu_6Sn_5$ in microbumps on ⟨1 1 1⟩ oriented and nanotwinned Cu

Han-wen Lin [a], Chia-ling Lu [a], Chien-min Liu [a], Chih Chen [a,*], Delphic Chen [b], Jui-Chao Kuo [b], K.N. Tu [c]

[a] Department of Materials Science & Engineering, National Chiao Tung University, Hsinchu, Taiwan, ROC
[b] Department of Materials Science & Engineering, National Cheng Kung University, Tainan, Taiwan, ROC
[c] Department of Materials Science and Engineering, University of California at Los Angeles, Los Angeles, CA 90095, USA

Received 22 September 2012; received in revised form 25 March 2013; accepted 26 April 2013
Available online 1 June 2013

**Abstract**

Anisotropic microstructure is becoming a critical issue in microbumps used in 3-D integrated circuit packaging. We report here an experimental approach for controlling the microstructure of η-$Cu_6Sn_5$ intermetallic compound in microbumps by using ⟨1 1 1⟩ oriented and nanotwinned Cu pads as the under-bump-metallization. By electroplating arrays of large numbers of ⟨1 1 1⟩ oriented and nanotwinned Cu pads and by electroplating the Sn2.3Ag solder on the pads, we form η-$Cu_6Sn_5$ in the reflow at 260 °C for 1 min. The η-$Cu_6Sn_5$ showed a highly preferential growth along the ⟨0 0 0 1⟩ direction. As reflow time is extended, the preferred texture of η-$Cu_6Sn_5$ changed to $\{2\,\bar{1}\,\bar{1}\,3\}$. The results indicate that we can control the uniform microstructure of η-$Cu_6Sn_5$ intermetallic by controlling the microstructure of the Cu under-bump-metallization.
© 2013 Acta Materialia Inc. Published by Elsevier Ltd. All rights reserved.

*Keywords:* Intermetallic compounds; Soldering; Copper

## 1. Introduction

Approaching the end of Moore's law for the large-scale integration of circuits in Si chip technology, a paradigm change from 2-D to 3-D integrated circuits (ICs) is occurring in the microelectronics industry. In essence, 3-D IC is a way to extend Moore's law by bringing packaging technology closer to chip technology. While Moore's law pertains to 2-D chip technology, we ask if there is a similar law for packaging technology; and if so, what is its future? On the basis of the scaling of the density of solder bumps on a chip surface, we find that there are at the least four more generations to go. Thus the future of chip technology can be extended if it is combined with packaging technology. For example, the diameter of a flip chip solder bump is about 100 μm today. We expect that it can be reduced to 1 μm, which will increase the density of bumps per unit area by four orders of magnitude. However, at the same time the volume of a solder bump is reduced by six orders of magnitude. This reduction becomes a yield and reliability issue from the point of view of the microstructure of the solder bump.

We consider a simpler case of reducing the bump diameter from 100 to 10 μm and assume a grain size of 10 μm. There is only 1 grain in the 10 μm diameter solder bump, but there are 1000 grains in the 100 μm diameter solder bump. In the latter case, we can assume a randomly oriented microstructure in every solder bump, so that all the solder bumps on a Si chip, over several hundred or thousands of them, have isotropic physical properties. In the former case, however, with 1 grain in a bump, we cannot do so and we must consider the anisotropic microstructure and properties of solder bumps—especially when we con-

* Corresponding author. Tel.: +886 3 5731814; fax: +886 3 5724727.
*E-mail address:* chih@mail.nctu.edu.tw (C. Chen).

1359-6454/$36.00 © 2013 Acta Materialia Inc. Published by Elsevier Ltd. All rights reserved.
http://dx.doi.org/10.1016/j.actamat.2013.04.056

sider early failure of solder bumps. Thus, microstructure control of small solder bumps becomes a critical issue. This consideration, when applied to 1 μm diameter solder microbumps, will be even more serious.

When a microbump has a very small number of grains, variation of grain orientation or microstructure can result in the microbump having a wide range of anisotropic properties, which is very undesirable from the point of view of yield and reliability. This is because certain grain orientations allow fast diffusion, and can induce early failure due to electromigration, for instance. Since there is a large number of microsolder bumps on a stack of chips in a 3-D IC, how to achieve a uniform microstructure with thousands of bumps on a chip is a critical issue for the future of 3-D IC manufacturing.

Controlling the microstructure of solder bumps is nontrivial because of reflow. Reflow means that the solder bump is melted to achieve chip-to-chip or chip-to-substrate joints. When a molten solder bump solidifies, it is very difficult to control the solidified microstructure. We report here that we can achieve a uniform microstructure of an array of a large number of microbumps by using ⟨1 1 1⟩ oriented and nanotwinned Cu as the under-bump-metallization (UBM) and have obtained a unidirectional growth of the intermetallic compound (IMC) in all the microbumps.

Why is IMC growth a concern for microbumps? While microbump volume has been reduced by 3–6 orders of magnitude, the reflow condition, typically 250 °C for 1 min for Pb-free solder, has not changed. This means that the IMC fraction in a microbump has increased dramatically. In fact, due to the need for several reflows in processing 3-D ICs and the need for solid-state aging because of reliability concerns, the entire microbump can become an IMC, and there will be no unreacted solder. This indicates that what we have discussed in the previous paragraph on microstructure control actually concerns the control required to achieve a uniform microstructure of IMC in thousands of microbumps. Of all the IMCs encountered in solder joints, the most important is $Cu_6Sn_5$ because of the widespread use of Sn-based Pb-free solder and Cu UBM.

Regarding microstructure control of IMCs, the unidirectional growth of η- and η′-$Cu_6Sn_5$ has been reported to occur on single-crystal Cu substrates. Suh et al. found preferential growth behavior of η′-$Cu_6Sn_5$ on (0 0 1) single-crystal Cu [1,2]. Zou et al. found a very strong texture of η′-$Cu_6Sn_5$ on (0 0 1), (0 1 1), (1 1 1) and (1 2 3) single-crystal Cu substrates [3,4]. On polycrystalline Cu, Kumar et al. have reported the formation of randomly oriented grains of $Cu_6Sn_5$ [5]. However, in microelectronic packaging technology, polycrystalline Cu UBM is typically produced by electroplating Cu metals on Si wafers, resulting in uncontrolled growth of IMC if the Cu UBM is polycrystalline.

We report here that the next best substrate to single-crystal Cu is ⟨1 1 1⟩ oriented and nanotwinned Cu, on which we have obtained unidirectional growth of IMC with tilt-type grain boundaries between the IMC grains. We prepared the ⟨1 1 1⟩ oriented and nanotwinned Cu UBM by electroplating. Sn2.3Ag was used as solder material. The orientation relationship between the oriented Cu and the oriented $Cu_6Sn_5$ has been examined and is reported here.

## 2. Experimental

To prepare the ⟨1 1 1⟩ oriented and nanotwinned Cu pads, we used $CuSO_4$-based electroplating solution with suitable additives. The current density was 10 or 80 mA $cm^{-2}$, and the rotation speed was set to about 800 rpm. Then, the Sn2.3Ag solder alloy was electroplated on the Cu.

To study IMC formation, the bumped Si die was reflowed at 260 °C for 1–5 min to grow $Cu_6Sn_5$. Then, after cooling in the air, the sample was ground by abrasive papers of #1000, #2000, and #4000 followed by polishing with $Al_2O_3$ powder of 1.0 and 0.3 μm. Finally, colloidal silica was used to remove the surface layer, which might be damaged during the polishing process. The morphology and the orientation image map in both cross-section view and top view after grinding and polishing were examined.

To study microsolder joints, we placed two bumped Si chips face-to-face and reflowed them for several minutes to make an array of microsolder joints between them. Cross-sections of the joined samples were prepared by grinding using #400, #1000, #2500 and #4000 abrasive papers after air cooling, and then polishing with 1 and 0.3 μm $Al_2O_3$ and colloidal silica. The focused ion beam (FIB) technique was adopted for cross-sectional observation. Images of solder joints were taken with a JEOL 7001 field emission scanning electron microscope. Orientation maps, inverse pole figures and pole figures were collected with an EDAX electron back-scatter diffraction (EBSD) system. It should be noted that a 3-D coordinate system was used to explain the orientation of grains in EBSD. In this paper, the direction out of the Cu pads was the normal direction (ND). The directions along the surface of the Cu pads were the rolling direction (RD) and the transverse direction (TD). These three directions are perpendicular to each other. X-ray diffraction (XRD) and transmission electron microscopy (TEM) were also adopted to verify the experimental results.

Monoclinic η′-$Cu_6Sn_5$ was found by Larsson et al. in 1994 [6]. Ever since then, the crystal structure of $Cu_6Sn_5$ has been controversial. Larsson has reported that the transformation temperature of $Cu_6Sn_5$ from η′-$Cu_6Sn_5$ to η-$Cu_6Sn_5$ is 186 °C. However, the reflow of solder joints involves heating up to 260 °C and cooling down to room temperature, and so the actual stable phase after joint formation is unclear. Ghosh and Asta reported the kinetics and energy of the η-$Cu_6Sn_5$ ↔ η′-$Cu_6Sn_5$ transformation [7]. Laurila et al. showed that the time required for the η to η′ transformation was insufficient with typical cooling rates in reflow [8,9]. Therefore, the η- $Cu_6Sn_5$ would remain as a metastable phase. Nogita et al. also made a

time–temperature–transformation diagram of the phase transformation of $Cu_6Sn_5$ and concluded that at under 70 °C the η-$Cu_6Sn_5$ in the joint could hardly transform into monoclinic structure [10]. Nogita et al. have also found that Ni has a stabilizing effect on the structure of η-$Cu_6Sn_5$ [11,12]. Schwingenschlögl et al. have further proven the stability of η-$Cu_6Sn_5$ by first-principles calculations [13]. Hence, the orientation relationship between η-$Cu_6Sn_5$ and Cu is important, as reported here.

## 3. Results

### 3.1. ⟨1 1 1⟩ oriented and nanotwinned Cu pad

Nanotwinned Cu was first reported by Lu et al., and possesses the unique combination of properties of exceptionally strong mechanical strength, good ductility and very little loss of electrical conductivity [14,15]. Nevertheless, the Cu grains with nanotwins were randomly oriented. In our experiments involving electroplating of Cu, the {1 1 1} twinning plane of the nanotwins is parallel to the Si wafer surface, and thus we have ⟨1 1 1⟩ oriented nanotwins rather than randomly oriented nanotwins. Furthermore, we can electroplate the oriented nanotwins in arrays of a large number of Cu pads. The diameter and thickness of each Cu pad are 100 and 20 μm, respectively.

To examine the orientation distribution of the nanotwins, we cut a flat surface on the Cu pads by FIB. The cut flat surface 50 μm long and 20 μm wide is shown in Fig. 1a. The square marked by the white dashed line in Fig. 1a indicates the area examined by EBSD (see Fig. 1b) and shows that the colors of Cu grains were all blue or blue purple in the orientation image map. This indicates that they all have approximately the same orientations. The inverse pole figure also shows the grain boundaries including twin boundaries on the top surface of the Cu pad. Referring to Fig. 1d showing the orientation of Cu, the orientation of all the Cu surface grains on the pads was confirmed to be either ⟨1 1 1⟩ or very close to it. Since the twinning plane is also the {1 1 1} plane of face-centered cubic Cu, we have obtained oriented and nanotwinned Cu.

The grain size of electroplated Cu is about 2–5 μm. The {1 1 1} pole figure in Fig. 1c proves that the pole at the normal direction of surface is almost parallel to ⟨1 1 1⟩. Fig. 1c suggests that the {1 1 1} pole of Cu is not exactly normal to the surface. However, the angular difference between the {1 1 1} pole of Cu and the ND of the Cu surface is less than 10°.

In addition, a TEM sample was prepared by FIB. Fig. 2a shows a bright-field image, enabling the grain of Cu to be observed. The diffraction patterns of three adjacent grains were taken separately and then superimposed on each other in Fig. 2b. This shows that these grains all had a pole of {1 1 1} and there were only a few degrees of rotation between different grains. The grain boundaries

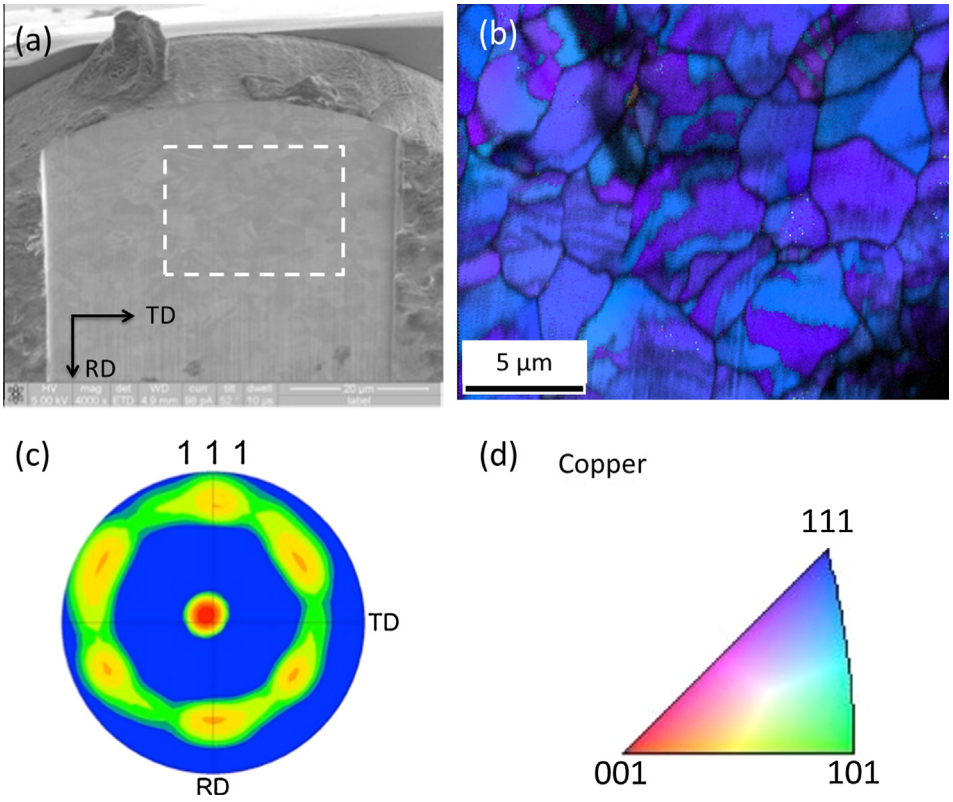


Fig. 1. (a) Plan-view of ⟨1 1 1⟩ unidirectional Cu Pads. (b) ND orientation map overlapped with image quality and grain boundaries. (c) The {1 1 1} pole figure, and (d) the reference figure (color coding).

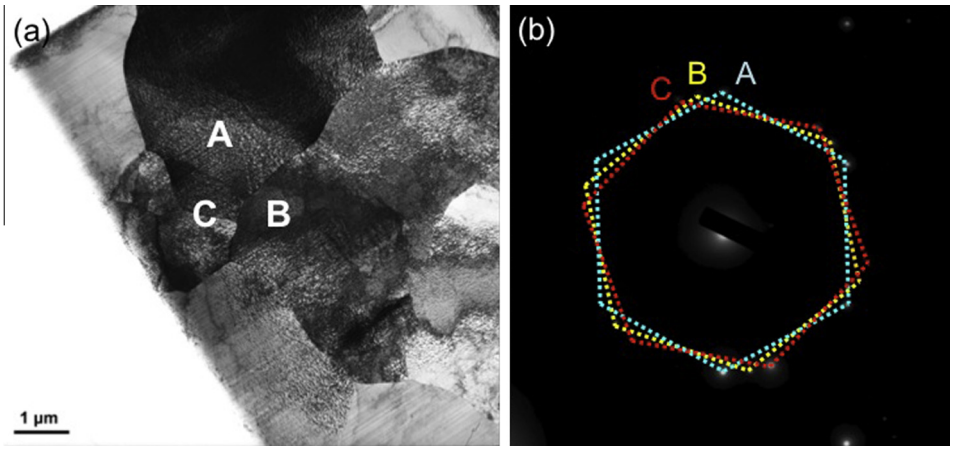


Fig. 2. (a) TEM image of Cu pads viewed from the top. (b) The diffraction patterns of three adjacent Cu grains.

between them are small-angle tilt-type grain boundaries. Although the Cu is still polycrystalline, the ⟨1 1 1⟩ preferred orientation is clear.

### 3.2. The preferential orientation relationship in solder bump structure

The Sn2.3Ag was electroplated on the ⟨1 1 1⟩ oriented and nanotwinned Cu pads. The reflow temperature was set to be 260 °C. After 1 min reflow, the chip was carefully mounted with low-temperature epoxy. The sample was ground and polished for cross-sectional examination. FIB was used to perform a final cut. Since Cu, $Cu_6Sn_5$ and SnAg solder were present, the advantage of adopting FIB is to make a cut precisely at the desired position and to a definitive thickness. Also, by performing the cut with a FIB, a strain-free surface can be revealed for all three phases.

Fig. 3a shows the FIB cross-section of a bump. The void inside the Cu pad was damaged during grinding and those inside the SnAg were due to flux. The red rectanglar area in Fig. 3a was carefully examined by EBSD. Fig. 3b–d show respectively the orientation image maps of Sn, $Cu_6Sn_5$ and Cu. The map shows the orientation of these phases in the direction perpendicular to the silicon chip surface. In other words, the orientation relationships along the direction of growth of these phases are shown in the figures. Once again, the color of the orientation image maps represents the orientation of the phases.

As displayed in Fig. 3d, the grain of Cu is columnar and the color of Cu is blue with some interlaced bands on it. Corresponding to the color coding in Fig. 3g, the orientation of ⟨1 1 1⟩ Cu was again confirmed. The interlaced bands are confirmed as nanotwins with only 5–20 nm twin spacing. The grain size of intermetallics is about 8 μm in width and 2 μm in height. Each IMC scallop has a uniform but different color, indicating that each scallop is a single grain of $Cu_6Sn_5$. Nevertheless these intermetallics are all shown in red and orange. This suggests that the intermetallics have a certain preferred orientation on the ⟨1 1 1⟩ Cu

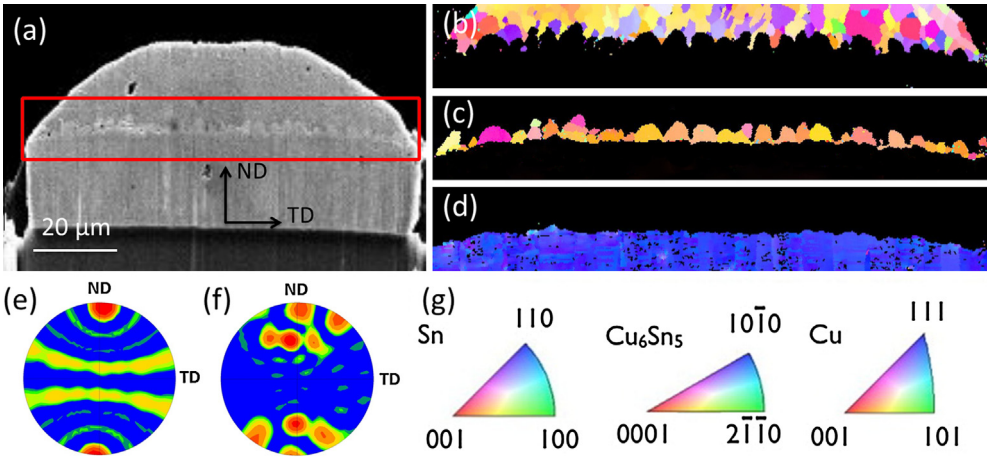


Fig. 3. (a) The cross-sectional area observed in the bump die structure. The ND orientation maps of (b) Sn, (c) $Cu_6Sn_5$ and (d) unidirectional Cu. (e) The {1 1 1} pole figure of Cu and (f) the {0 0 0 1} pole figure of η-$Cu_6Sn_5$. (g) The reference figure for Sn, $Cu_6Sn_5$ and Cu. (For interpretation of the references to color in this figure legend, the reader is referred to the web version of this article.)

pad. By reference to Fig. 3g, the orientation of intermetallics along ND is close to ⟨0001⟩. To confirm this result, we examine the pole figure of {0001} of intermetallics as well as that of {111} Cu. In Fig. 3e, the {111} pole figure of Cu showed that the pole was mostly aligned with the ND. Combined with Fig. 3f, the {0001} pole of $Cu_6Sn_5$ was found also to center along the ND. As mentioned in Section 3.1, the {111} pole of Cu has a small distribution around the normal of the Si surface, and hence the pole figure of both Cu and $Cu_6Sn_5$ showed some leaning behavior. The amount of leaning is just a few degrees. With these results, the orientation relationship between the nanotwinned Cu and η-$Cu_6Sn_5$ can be clearly identified as: $\{111\}_{nt\text{-}Cu}\|\{0001\}_{Cu6Sn5}$. This preferred growth relationship is credible because the intermetallic contacted the Cu directly with little formation of $Cu_3Sn$ in between them because the reflow time was only 1 min.

### 3.3. Effect of reflow time on the orientation relationship

To obtain a general view of the orientation of every intermetallic grain on a single Cu pad, the surface of the intermetallic was revealed by grinding and polishing the top surface. Since the intermetallics in Section 3.2 were too small and hard to be reached precisely when ground by human hands, the sample was further reflowed for 4 min to make the intermetallic grains larger.

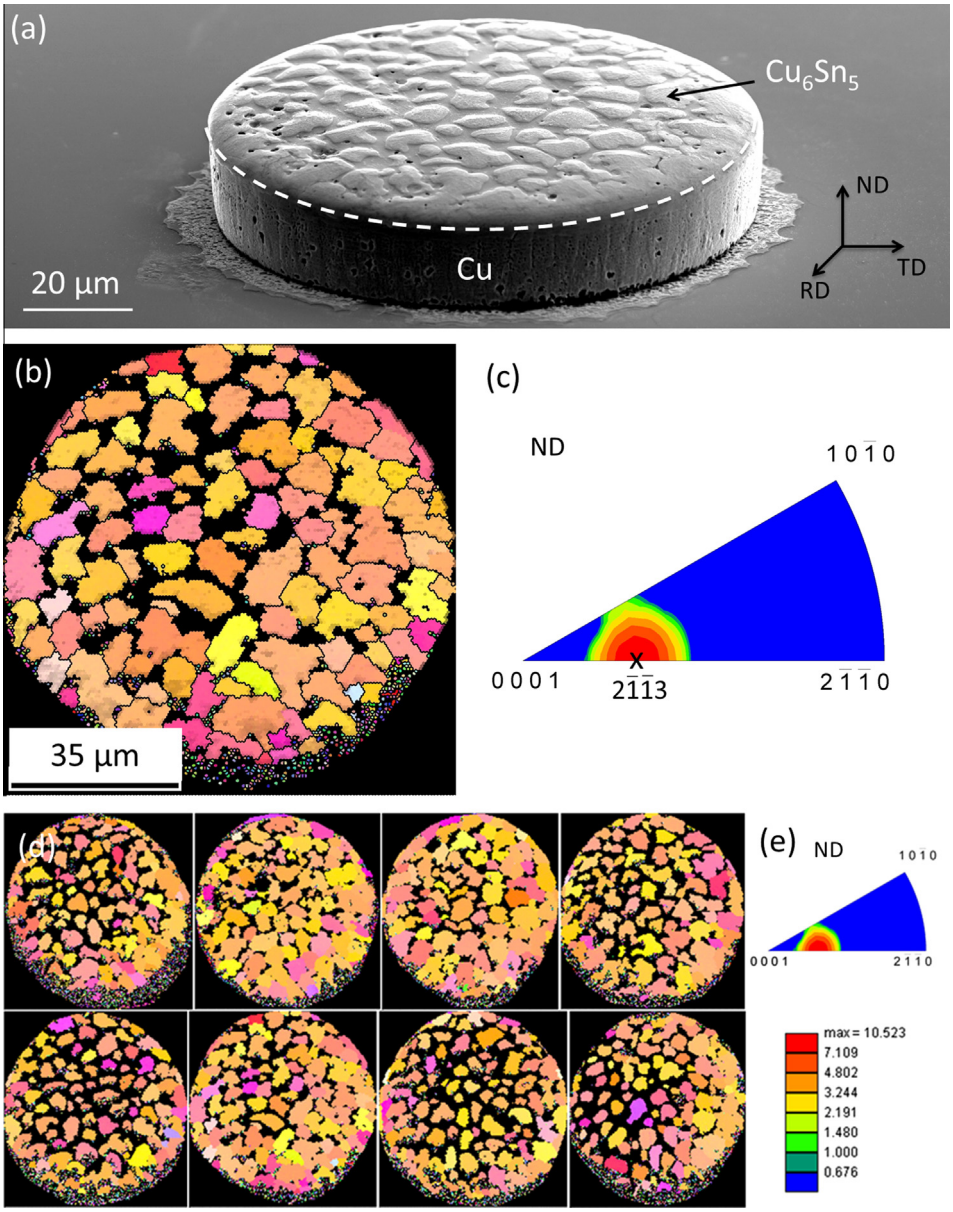


Fig. 4. (a) SEM image from the plan view of $Cu_6Sn_5$. (b) The ND orientation map of $Cu_6Sn_5$, and (c) the ND inverse pole figure of $Cu_6Sn_5$. (d) ND orientation maps of $Cu_6Sn_5$ IMCs on eight microbumps, and (e) the ND inverse pole figure for the IMCs in (d). Refer to the color coding in Fig. 3g. (For interpretation of the references to color in this figure legend, the reader is referred to the web version of this article.)

Fig. 4a shows the SEM image of a Cu pad with Sn and $Cu_6Sn_5$ on it. The islands on the Cu pad were $Cu_6Sn_5$ formed during reflow; between them was the residual Sn phase. With the ND orientation map of Fig. 4b, the colors of intermetallics were purple, orange and yellow. It should be noted that some noise signals are shown on the peripheral area of the figure. When we revealed the plan-view of the intermetallic by grinding from the top of solder ball, the shape of hemisphere makes the peripheral area bumpy, which will cause some noise around the circumference of the pad.

These samples differ in a number of respects from those reflowed for only 1 min. First, more $Cu_6Sn_5$ grains appear yellow in Fig. 4b. This indicates that the preferred texture of intermetallics has changed from $\{0\,0\,0\,1\}$ to $\{2\,\bar{1}\,\bar{1}\,0\}$. The ND inverse pole figure (see Fig. 4c) shows that the major texture of the intermetallic has been changed to $\{2\,\bar{1}\,\bar{1}\,3\}$. In this study, dozens of microbumps with $\{1\,1\,1\}$ nanotwinned Cu pads were examined by EBSD. Fig. 4d shows the ND orientation maps for the $Cu_6Sn_5$ IMCs on eight microbumps. All of them had similar preferred texture. By merging the $Cu_6Sn_5$ orientation data from all these microbumps, we can construct the ND inverse pole figure (see Fig. 4e), which is obtained from the EBSD data in Fig. 4d. The ND preferred texture in Fig. 4d is almost identical to that in Fig. 4b, indicating that the $Cu_6Sn_5$ on every bump has the same preferred growth behavior in the ND. There are reports in the literature which show that the morphology of $Cu_6Sn_5$ would change after reflow at higher temperatures or for longer times [1,2]. Another intermetallic, $Cu_3Sn$, starts to grow at the interface between Cu and $Cu_6Sn_5$. The formation of $Cu_3Sn$ would break the preferential growth relationship between $Cu_6Sn_5$ and Cu because the $Cu_6Sn_5$ would then grow on $Cu_3Sn$, instead of on Cu.

### 3.4. The preferential orientation of IMC in a solder joint

The preferential relationship between $Cu_6Sn_5$ and Cu is important in real packaging solder joints. The solder joints were fabricated by joining two bump-on-dies together. We flipped one chip with the Sn2.3Ag solder and the oriented and nanotwinned Cu pads on another chip, and these were then reflowed at 260 °C for 3 min in total to make the microsolder joints. The sample was then ground and polished, and finally cut by FIB.

Fig. 5a shows the ND orientation maps of the joints. The Cu pad is blue, because it has an oriented microstructure from the bottom to the top. By reference to Fig. 3g it can be confirmed that the entire column was all $\langle 1\,1\,1\rangle$ oriented and contained nanotwins in each grain. There were some grains showing colors other than blue at the bottom. This might be a transition region from the seed layer to the nanotwinned Cu. The scallop-type $Cu_6Sn_5$ appeared in red, orange and yellow. Fig. 5b shows the two colored layers of $Cu_6Sn_5$ separately. The middle part in Fig. 5b is the remaining Sn2.3Ag. As noted in the previous section, the orientation of Cu along the ND was $\langle 1\,1\,1\rangle$ and that of $Cu_6Sn_5$ was close to $\langle 0\,0\,0\,1\rangle$.

When we reflowed the joint for 4 min, some of the intermetallic from the top and from the bottom contacted each other and seemed to merge together as shown in Fig. 6a. It should be noted that an unequal growth rate of $Cu_6Sn_5$ on each side of Cu pad was observed. This is mainly because of the unequal Cu flux during reflow. This phenomenon has been reported in our previous study [16]. In addition, the orientation map of $Cu_6Sn_5$ in Fig. 6a shows that the two intermetallic grains from the top and the bottom became one single grain as soon as they come into contact with each other. This seems to be a unique property of $Cu_6Sn_5$, which has a very fast grain growth rate or ripening

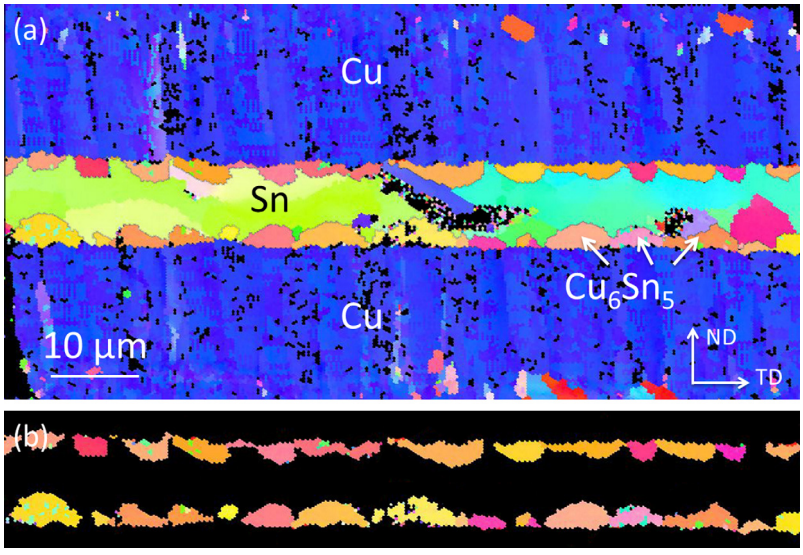


Fig. 5. The ND orientation maps of (a) the solder joints reflowed at 260 °C for 3 min, and (b) the two colored layers of $Cu_6Sn_5$. Refer to the color coding in Fig. 3g. (For interpretation of the references to color in this figure legend, the reader is referred to the web version of this article.)

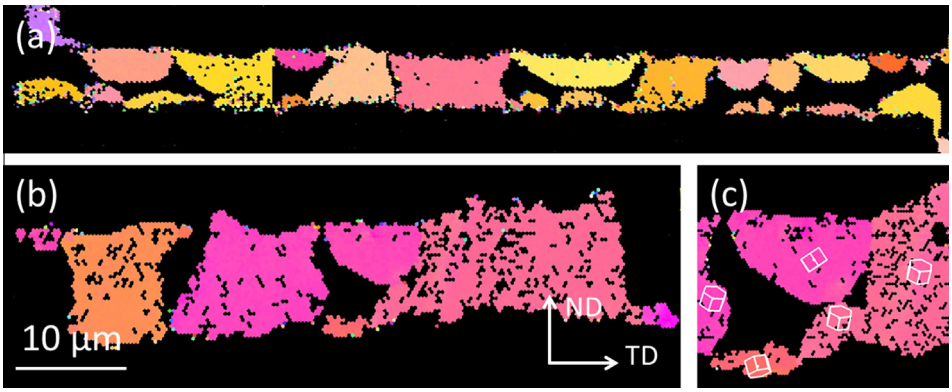


Fig. 6. The ND orientation maps of η-$Cu_6Sn_5$ after the solder joints were reflowed at 260 °C for (a) 4 min and (b) 5 min; (c) magnified image of (b) with grain orientations indicated by the tiny hexagonal unit cells. Refer to the color coding in Fig. 3g. (For interpretation of the references to color in this figure legend, the reader is referred to the web version of this article.)

rate. We note that the intermetallic grains were small after 3 min of reflow. Hence, they needed to grow first and then they can contact with each other. The reaction when they are in contact with each other must be very fast since the transition can be finished in an additional minute, from 3 to 4 min, at 260 °C.

The reflow time was further increased for an additional minute for another joint, giving a total reflow time of 5 min. The results are shown in Fig. 6b. Most of the intermetallics were merged together. The orientations of these intermetallics were still close to ⟨0001⟩ in the ND. The magnified image in Fig. 6c shows tiny white hexagonal unit cells that represent the exact orientation of each grain of η-$Cu_6Sn_5$. As illustrated by this figure, the {0001} planes of the hexagons were almost parallel to the Cu pads whether they were at the top chip or at the bottom chip. All the c-axes of these hexagonal unit cells lie along the direction perpendicular to the Cu pads. When two grains start to merge together, their orientations seem to merge too.

## 4. Discussion

### 4.1. Coherence between {0001} η-$Cu_6Sn_5$ and {111} Cu

There have been many reports about the preferential growth of η′-$Cu_6Sn_5$ on Cu. The crystal structure of η′-$Cu_6Sn_5$ is monoclinic ($C_2/c$, $a = 11.022$ Å, $b = 7.282$ Å, $c = 9.827$ Å, $\beta = 98.84°$). However, in Section 1 we have noted that the η-$Cu_6Sn_5$ would be the phase present in solder joints. In this study, we mainly focused on the preferential growth behavior between η-$Cu_6Sn_5$ ($P63/mmc$, $a = 4.2032$ Å, $c = 5.1107$ Å) and the ⟨111⟩ oriented Cu. The crystal structure of Cu is face-centered cubic with $a = b = c = 3.615$ Å.

Our experimental results in Section 3.2 indicate that the {0001} plane of η-$Cu_6Sn_5$ is parallel to the {111} plane of Cu during the early stages of reflow. After superimposing the Cu atoms of these two planes, we could hardly found any two directions that are of lower lattice mismatch through the whole plane of contact. Thus it is difficult to explain this coherent relationship in terms of lattice matching. Nevertheless, in this study, although the Cu pads were made to have a ⟨111⟩ preferred orientation and additionally the surfaces of the Cu pads were {111} planes, these pads still possessed a polycrystalline textured surface. Fig. 2b has already proven that there were rotation or tilt-type behaviors between adjacent Cu grains. Hence, the arrangement of Cu atoms on the surface is not complete identical to single-crystal Cu. Moreover, the grain size of $Cu_6Sn_5$ was larger than that of columnar Cu grains, indicating that the η-$Cu_6Sn_5$ must grow on several grains of Cu. Therefore it is not possible to have a low lattice mismatch across the entire interface.

The soldering reaction between Cu and Sn forms $Cu_6Sn_5$. It is obvious that the bond energy between Cu and Sn must be lower than that between Cu and Cu [11]. We should also discuss the coherence between the Sn in the η-$Cu_6Sn_5$ and the Cu in the ⟨111⟩ oriented Cu. However, it is also hard to achieve coherence since Sn atoms are more difficult to located in the hexagonal lattice of $Cu_6Sn_5$. The Sn atoms in the hexagonal $Cu_6Sn_5$ lie on the plane close to $\{2\,\bar{1}\,\bar{1}\,3\}$. Hence, we can now only conclude that because the {0001} plane of η-$Cu_6Sn_5$ and the {111} plane of Cu are the most densely packed atomic planes in both lattices, there is a high density of Cu–Sn bonds across the interface which lowers the interfacial energy.

### 4.2. The change in orientation of the intermetallic with reflow time

Inverse pole figures were constructed to show the orientation of η-$Cu_6Sn_5$ with time in Fig. 7. At the early stage of reflow, up to 3 min, the η-$Cu_6Sn_5$s were mainly ⟨0001⟩ orientated in Fig. 7a and b. When the reflow time was extended to 4 min, another orientation was found to play a more important role, as shown in Fig. 7c. And finally, the ⟨0001⟩ orientated $Cu_6Sn_5$ disappears on the joint reflowed for 5 min (Fig. 7d). The texture of η-$Cu_6Sn_5$ kept at 260 °C for 5 min lies between {0001} and $\{2\,\bar{1}\,\bar{1}\,0\}$. By

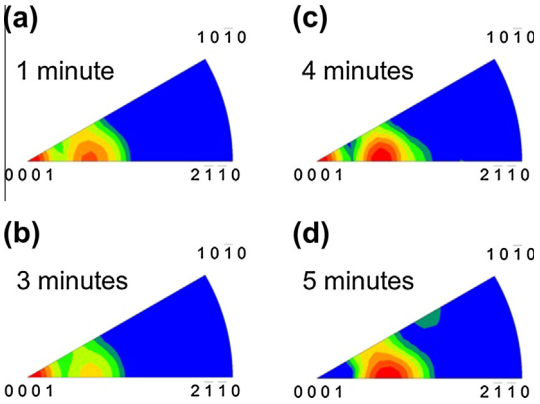


Fig. 7. The ND inverse pole figure of η-$Cu_6Sn_5$ after the solder joints were kept at 260 °C for (a) 1 min, (b) 3 min, (c) 4 min and (d) 5 min.

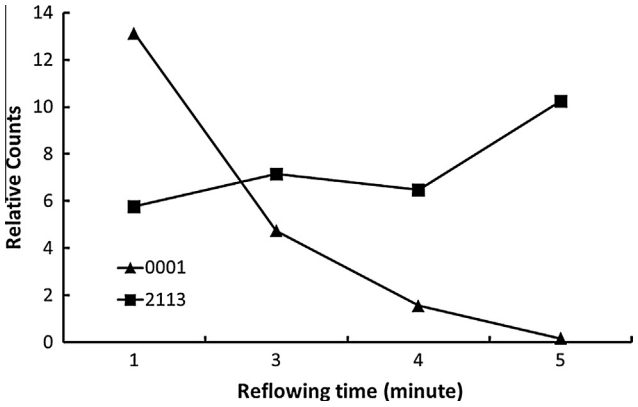


Fig. 8. The trend of orientation change of η-$Cu_6Sn_5$.

using the software of the analysis system, we can define this new texture as $\{2\,\bar{1}\,\bar{1}\,3\}$.

Fig. 7 clearly shows the changes in texture with time. We can read the relative counts of $\{0001\}$ and $\{2\,\bar{1}\,\bar{1}\,3\}$ at each stage of reflow and make a statistical analyses. The results are shown in Table 1 and Fig. 8. We note that the relative counts are defined as the intensity of specific pole divided by the intensity of any random orientations (in units of "times random").

Table 1 shows the relative counts of each pole for various reflow durations. For 1 min reflow, the relative counts of $\{0001\}$ are 13.13 and that of $\{2\,\bar{1}\,\bar{1}\,3\}$ are 5.77. As the reflow time is extended, the intensity of $\{0001\}$ decreased down to only 0.17 and that of $\{2\,\bar{1}\,\bar{1}\,3\}$ increased up to 10.24. In Fig. 8, the trends of orientation change are shown. It is very clear that the intensity of $\{0001\}$ decreases rapidly after reflow for 3 min. And the texture of $\{2\,\bar{1}\,\bar{1}\,3\}$ increased slowly at the early stage of reflow and rapidly between 4 and 5 min of reflow.

The reason why the preferred orientation of η-$Cu_6Sn_5$ on $\{1\,1\,1\}$ Cu might change is due to the formation of $Cu_3Sn$. During the early stages of reflow, the η-$Cu_6Sn_5$ forms directly on Cu, making it a lower energy state by stacking its $\{0\,0\,0\,1\}$ plane on $\{1\,1\,1\}$ Cu. However, as the time of reflow is extended, the η-$Cu_6Sn_5$ grows larger and blocks the diffusion path of Cu. At the same time, $Cu_3Sn$ forms at the interface between $Cu_6Sn_5$ and the Cu. Subsequently, the formation of η-$Cu_6Sn_5$ occurs not on the Cu but on the $Cu_3Sn$ instead.

The mechanism of this transformation, including how the $Cu_6Sn_5$ is coherent with $Cu_3Sn$ and how the $Cu_6Sn_5$ changes its orientation in solids, is still unclear. Some previous studies have shown that the morphology of $Cu_6Sn_5$ did change with reflow time. The formation of $Cu_3Sn$ would break the coherence relationship between η-$Cu_6Sn_5$ and single-crystal Cu. None of this earlier research has shown the orientation of $Cu_6Sn_5$ after the surface morphology had disappeared. In this study, we showed that the preferential growth of scallop-type $Cu_6Sn_5$ continued even after the formation of $Cu_3Sn$. However, we believe that subsequent adequate thermal annealing would change the orientation of these intermetallics again. This is a much more complicated reaction since it involves not only the crystallization behavior of $Cu_6Sn_5$ on $Cu_3Sn$, but also the phase transformation for $Cu_6Sn_5$ from η to η′. Further study is required to establish the entire mechanism. However, the $\{1\,1\,1\}$ Cu is able to control the microstructure of $Cu_6Sn_5$ during the fabrication stage and the early stages of use. Therefore, the properties of each microbump can be controlled.

Table 1
Relative counts of $(0\,0\,0\,1)$ and $(2\,\bar{1}\,\bar{1}\,3)$ at each stage of reflowing.

| | 0001 | $2\bar{1}\bar{1}3$ |
|---|---|---|
| 1 min | 13.13 | 5.77 |
| 3 min | 4.75 | 7.15 |
| 4 min | 1.60 | 6.47 |
| 5 min | 0.17 | 10.24 |

### 4.3. Effect of ⟨1 1 1⟩ oriented Cu pads on the orientation of $Cu_6Sn_5$

In electroplating, factors including solution base, current (including densities and alternating or direct current), temperature and additives can affect the quality of electroplated metals. To examine the effect of Cu pads on the growth of preferred orientation of η-$Cu_6Sn_5$, other chips with Cu pads electroplated with various current densities were prepared. It should be noted that other electroplating parameters were fixed and the pattern of Cu pads are similar on all the chips.

Fig. 9 shows the results for the Cu pads electroplated with various current densities. In Fig. 9a, the ion image was taken after the making a final cut by FIB. The Cu pad was electroplated with a lower current density at 1 ASD. The grain structure of Cu resembles that of typical electroplated Cu. There are some twin boundaries in it, though most of these are microtwins, with a few being nanotwins. The columnar grain appeared sometimes by chance. XRD analysis shows these pads still had large

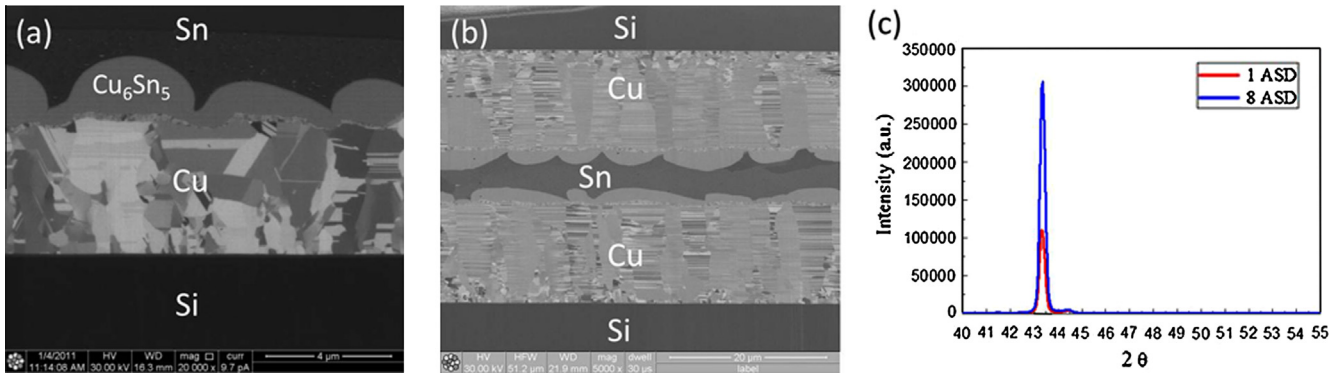


Fig. 9. The cross-sectional ion image of Cu pads electroplated with a current density of (a) 1 ASD and (b) 8 ASD. (c) The XRD results of Cu pads electroplated with current densities of 1 and 8 ASD.

counts of about 100,000 about the {1 1 1} peak of Cu, as shown in Fig. 9c. In our experiments, we have adopted a chip with Cu pads electroplated at a higher current density of 8 ASD. As shown in Fig. 9b, the Cu grains were all columnar throughout the entire pad. Each grain contains a high density of nanotwins. The diameter of each column was 2–5 μm. Fig. 9c shows the XRD results of these Cu pads; there were more than 300,000 counts of the {1 1 1} peak of Cu. In our other electroplating process, we have adopted several settings of much higher and lower current densities. The best result we had was similar to that shown in Fig. 9b. Therefore, the optimum current density of 8 ASD was adopted to produce a ⟨1 1 1⟩ oriented and nanotwinned Cu.

After the Cu pads were produced, the Sn2.3Ag was then electroplated on them. These chips were reflowed at 260 °C for up to 5 min to grow the intermetallic. Fig. 10a and b show respectively the orientation image map and the inverse pole figures of the $Cu_6Sn_5$ on the Cu pads electroplated at 1 ASD. Fig. 10c and d show respectively the results for the $Cu_6Sn_5$ on the Cu pads electroplated at 8 ASD. In Fig. 10a, the colors of $Cu_6Sn_5$ are more divergent. There are now several grains blue and green, and the color divergence is greater than that in Fig. 10c. In addition, the inverse pole figures in Fig. 10b and d show that the η-$Cu_6Sn_5$ was more concentrated on the oriented Cu pads of better quality. This means that the $Cu_6Sn_5$ grains had no strong preferred orientations on the Cu pad electroplated by 1 ASD. Again, after being reflowed at 260 °C for 5 min, the texture of η-$Cu_6Sn_5$ was centralized at {2 $\bar{1}$ $\bar{1}$ 3}. Conversely, the orientations of $Cu_6Sn_5$ were more random on the Cu pad electroplated with lower current densities.

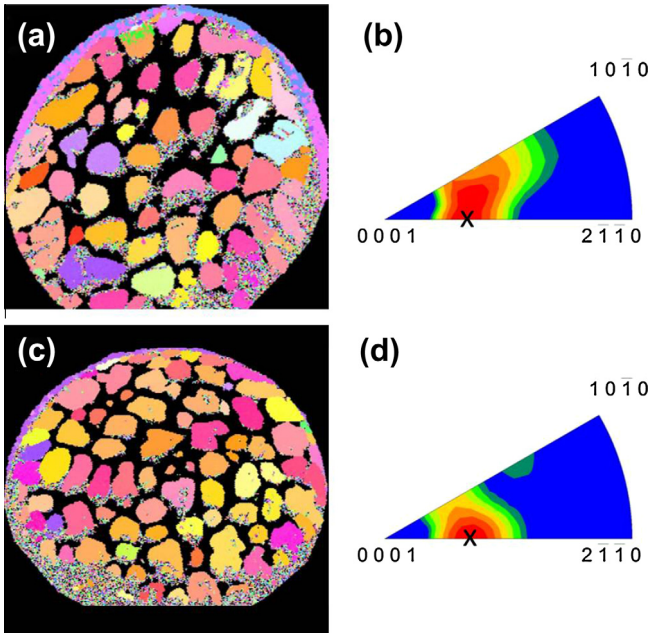


Fig. 10. (a) The orientation image map and (b) the inverse pole figure of η-$Cu_6Sn_5$ on 1 ASD Cu pads. (c) The orientation image map and (d) the inverse pole figure of η-$Cu_6Sn_5$ on 8 ASD Cu pads.

## 5. Conclusions

⟨1 1 1⟩ oriented and nanotwinned Cu has been produced by electroplating. The Cu grains are columnar with a diameter of about 2–5 μm. After electroplating Sn2.3Ag on the oriented Cu pads and followed by reflow at 260 °C, the η-$Cu_6Sn_5$ showed a preferential growth of {0 0 0 1} texture at the early state of growth. As the time of reflow is extended, the preferred texture of $Cu_6Sn_5$ changes to {2 $\bar{1}$ $\bar{1}$ 3}. Since the ⟨1 1 1⟩ oriented and nanotwinned Cu was polycrystalline, the coherence between the η-$Cu_6Sn_5$ and the Cu most likely is achieved via a high density of Cu–Sn bonds across the interface between them. Electroplating parameters affect the quality of oriented Cu and therefore would affect the preferential growth of $Cu_6Sn_5$. Being able to control the electroplating of ⟨1 1 1⟩ oriented and nanotwinned Cu means that we can control the orientation and in turn the microstructure of the intermetallic in microsolder joints.

## Acknowledgement

The authors gratefully acknowledge the financial support of the National Science Council of the Republic of China (Grant No. NSC 101-2628-E-009-017-MY3).

## References

[1] Suh JO, Tu KN, Tamura N. Appl Phys Lett 2007;91:051907.
[2] Suh JO, Tu KN, Tamura N. J Appl Phys 2007;102:063511.
[3] Zou HF, Yang HJ, Zhang ZF. Acta Mater 2008;56:2649.
[4] Zou HF, Yang HJ, Zhang ZF. J Appl Phys 2009;106:113512.
[5] Kumar V, Fang ZZ, Liang J, Dariavach N. Metall Mater Trans A 2006;37:2505.
[6] Larsson AK, Stenberg L, Lidin S. Acta Cryst 1994;B50:636.
[7] Ghosh G, Asta M. J Mater Res 2005;20:3102.
[8] Laurila T, Vuorinen V, Paulasto-Kröckel M. Mater Sci Eng R 2010;68:1.
[9] Laurila T, Vuorinen V, Kivilahti JK. Mater Sci Eng R 2005;49:1.
[10] Nogita K, Gourlay CM, McDonald SD, Wu YQ, Read J, Gu QF. Scripta Mater 2011;65:922.
[11] Nogita K. Intermetallics 2010;18:145.
[12] Nogita K, Nishimura T. Scripta Mater 2008;59:191.
[13] Schwingenschlögl U, Paola CD, Nogita K, Gourlay CM. Appl Phys Lett 2010;96:061908.
[14] Lu L, Shen Y, Chen X, Qian L, Lu K. Science 2004;304:422.
[15] Lu L, Chen X, Huang X, Lu K. Science 2009;323:607.
[16] Kuo MY, Lin CK, Chen C, Tu KN. Intermetallics 2012;29:155.